This work is on a Creative Commons Attribution 4.0 International (CC BY 4.0) license, https://creativecommons.org/licenses/by/4.0/. Access to this work was provided by the University of Maryland, Baltimore County (UMBC) ScholarWorks@UMBC digital repository on the Maryland Shared Open Access (MD-SOAR) platform.

Please provide feedback Please support the ScholarWorks@UMBC repository by emailing scholarworks-group@umbc.edu and telling us what having access to this work means to you and why it's important to you. Thank you.

Determining planetary boundary layer height by micro-pulse lidar with validation by UAV measurements

Yueh-Chen Wang[1], Sheng-Hsiang Wang[1,2 *], Jasper R. Lewis[3], Shuenn-Chin Chang[4,5], Stephen M. Griffith[1]

[1] Department of Atmospheric Sciences, National Central University, Taoyuan, Taiwan

[2] Center for Environmental Monitoring and Technology, National Central University, Taoyuan, Taiwan

[3] University of Maryland Baltimore County, Maryland, USA

[4] Environmental Protection Administration, Taipei, Taiwan

[5] School of Public Health, National Defense Medical Center, Taipei, Taiwan

To be submitted to Aerosol and Air Quality Research

*Corresponding Author:

Tel: +886-3-422-7151 ext 65527

E-mail address: shenghsiang.wang@gmail.com; carlo@g.ncu.edu.tw

ACCEPTED MANUSCRIPT

Abstract

Planetary boundary layer height (PBLH) is often used to characterize the structure of the lower atmosphere. Aerosol lidar, a ground-based remote sensing method, provides the vertical distribution of aerosol at a high temporal resolution observation data, from which, the PBL structure and the position of the PBL top can be comprehensively studied. PBLH determination with lidar data depends primarily on the characteristic turbulent motions in the atmosphere and the geophysical location. However, lidar determination of PBLH over densely populated subtropical locations has rarely been discussed; thus, developing retrieval techniques suitable to these areas is necessary. In this study, four PBLH determination methods (Gradient, δ–threshold, Haar wavelet transform, and hybrid image processing) are applied to estimate the PBLH from lidar observations over an urban area in East Asia, and one – the Gradient method – relied on potential temperature measurements from an unmanned aerial vehicle (UAV) flights to validate our results. Our results indicate that a combination of the gradient method and δ-threshold method can provide better results, in terms of diurnal pattern, than using either method individually. Furthermore, the Haar wavelet and the Hybrid image processing can detect the PBL development comparably well, but both methods are dependent on their initial conditions and optimized algorithm settings. In addition, the accompanying UAV observations are conclusively shown to have a high degree of efficacy for validating the lidar data. This research highlights that a combination of PBLH determination methods can better describe the PBLH evolution throughout a day in some cases, while in others less common determination methods are proving useful, and a suite of retrieval methods should still be explored for precisely mapping the PBL in densely populated subtropical areas.

Keywords: micro-pulse lidar (MPL); unmanned aerial vehicle (UAV); planetary boundary layer (PBL)

ACCEPTED MANUSCRIPT

INTRODUCTION

The planetary boundary layer (PBL), or atmospheric boundary layer (ABL), is part of the troposphere directly influenced by surface forcing (Stull, 1988). To investigate the structure of the PBL, vertically-resolved observations from remote sensing technologies, such as high towers, balloons, lidar, wind profilers etc., are widely used (Hellmann et al., 1915; Peppler, 1921; Mildner, 1932; Davis et al., 2000; Lewis et al., 2013). Aerosol lidar is a mainstream technology which using aerosol as tracer to illustrate PBL structure and further apply to air quality study.

Micro-Pulse Lidar (MPL) is a ground-based, autonomous and compact remote sensing technology used for aerosol and thin cloud vertical profiling throughout the atmosphere (Spinhirne, 1993; Welton et al. 2002). MPL is highly sensitive to aerosol scattering and utilizes dual-polarization elastic-backscatter lidar, based on Rayleigh and Mie scattering theory. MPL retrieves the aerosol scattering coefficient, translatable to a mass concentration or often to the normalized relative backscatter (NRB) signal, and illustrates the aerosol distribution clearly at distinguishable levels up to 25 km under ideal conditions, especially at daytime when the signal-to-noise ratio is the highest (He et al., 2012). MPL also provides volume depolarization ratio data, a measurement of aerosol symmetry (Flynn et al, 2007). Aerosols within the PBL are usually capped by an inversion layer, while significantly lower aerosol concentrations are observed in the free troposphere. Therefore, the intensity of the lidar backscatter signals reduce significantly from

ACCEPTED MANUSCRIPT

the top of the PBL to the free troposphere, and these dramatic changes are used to estimate the planetary boundary layer height (PBLH) (Gaudio et al., 2015).

MPL data are widely used to determine the PBLH because of its ability to monitor aerosol backscatter and vertically profile at a high temporal resolution. To this end, several groups have developed a variety of PBLH retrieval techniques from the lidar NRB/ backscatter signals (Davis et al., 2000; Lucchese and Mitra, 2001; Brooks, 2003; Müller et al., 2010; Bravo-Aranda et al., 2017; Li et al., 2017), with most of the methods able to capture general trends in the convective daytime PBL development. Although, lidar is best suited to determine daytime PBLH (i.e. mixing layer height), certain nighttime conditions are still suitable for this type of analysis, including stable nocturnal conditions. However, due to residual layers and near-field measurement limitations, resolving nocturnal PBLH trends still has a high associated uncertainty. For instance, Li et al. (2007) found that the gradient method and idealized backscatter method, both lidar methods for PBLH determination, were suitable in high signal-to-noise ratio conditions, but failed at low signal-to-noise ratio conditions whether in the daytime or nighttime. Thus, there is significant room to improve the existing algorithms for optimizing daytime determinations and realizing nighttime determinations. Other retrieval methods include combining WCT (wavelet covariance transform) (Berkoff et al., 2003; Bravo-Aranda et al., 2017) and basic image analysis techniques to remove the influence of clouds and residual layers, which has correlated well with

ACCEPTED MANUSCRIPT

sounding observations and modelled PBLH from GEOS-5 (The Goddard Earth Observing System Model, Version 5) (Lewis et al., 2013). However, different forms of wavelet analysis, for example, Haar wavelet and Mexican Hat wavelet, have been found to be highly dependent on different initial values or different initial amplitudes.

Determination of PBLH is dependent on retrieval methods affected by geophysical locations, of which the optimal method is still debated in the literature. Therefore, the objective of this study is to develop retrieval techniques suitable for PBLH detection in densely populated subtropical locations. In contrast to previous studies using the NRB for PBLH retrieval, we used the depolarization ratio (δ) for PBLH retrieval as has been done in a few recent studies. De Tomasi et al. (2011) used δ to discuss how the PBL differences between a continental area to a coastal area. Bravo-Aranda et al. (2017) used wavelet analysis to compare with PBLH derived from lidar depolarization ratio and microwave radiometer data, and found the former was consistently shallower during the daytime, but at nighttime there was better agreement. The δ is the ratio of the cross-polarized NRB signals and the total (both cross-polarized and co-polarized) NRB signals, and its value implies particle shapes or nonsphericity of particles. In addition, using δ to tracing the PBLH, is a useful parameter to distinguish between aerosol types such as dust, anthropogenic, and fresh/aged aerosols. Under a well-mixing PBL condition, locally assembled particles populate within PBL with similar δ values. The MPL measurements provide useful

ACCEPTED MANUSCRIPT

information with a high temporal and special resolution which independently confirms the PBLH estimation. Furthermore, in this study, UAV (unmanned aerial vehicle) is utilized as an independent PBLH determination method and validation for the lidar methods. PBL development characteristics are dependent on geophysical location. The purpose of this study is to find retrieval techniques suitable for PBLH detection in densely populated subtropical locations; this paper focuses primarily on retrieval methods suitable over urban areas in East Asia.

This article is organized as follows. Descriptions of the experiment and PBLH determination methods are described in methods section. Results comparing several PBLH determination methods and validation by UAV observation are presented in results and discussion section. Finally, conclusions and future prospects are presented in last section.

METHODS

Experiment and Instrumentation

We carried out this experiment nearby the Taiwan CWB (Central Weather Bureau) sounding station in Banqiao, New Taipei City from June 21 – September 19, 2017 (Fig. 1). The total population of New Taipei City is nearly four million, and Banqiao is the most populous district (Fig. 1(a)). Banqiao is located on flat terrain near the western boundary of the Taipei basin (Fig. 1(b)), which also includes much of Taipei City, the capital. The southwest monsoon prevails in

ACCEPTED MANUSCRIPT

the summer-months, but primarily the weather in New Taipei City is affected by the basin's topography. Furthermore, the mountains around the Taipei basin lock the hot air mass near the surface, and therefore the temperature is usually higher than the surrounding area, enhancing the heat island effect. As a result, the main source of pollution in Banqiao during the summertime is from local anthropogenic emissions. Days without influence from long-range transport were chosen in order to test the PBLH retrieval methods under only local influence and compared across similar conditions. Observational data from MPL and UAV were used in this study, and aerosol layers at different heights were distinguished through lidar observation profiles. During the long-range transport or transboundary events, the NRB signal or the depolarization ratio of this layer will be higher than the surrounding air mass and remain aloft.

Our MPL system was manufactured by Sigma Space Corporation (now Droplet Measurement Technologies), and the specifications are shown in Table 1. For the experiment, the MPL was installed at the Banqiao sounding station. We programmed the MPL for a vertical resolution of 75 meters and temporal resolution of 1 minute. Routine maintenance was carried out following the guidance of MPLNET (The NASA Micro-Pulse Lidar Network), including monthly dark count and after-pulse calibrations. However, instead of using the operational data provided by MPLNET, the raw data were processed locally based on Welton et al (2002) and our Level 1 data,

ACCEPTED MANUSCRIPT

including NRB and volume depolarization ratio (δ), followed the methods described by the previous studies (Welton et al., 2002; Flynna et al., 2007; Welton et al., 2018).

In this study, we used MPL observations and UAV measurements to characterize the structure of the PBL including the location of the PBL top. The UAV measurements were used as a general validation of the MPL-derived PBLH determination methods over the denoted area. In summertime, the PBLH can easily reach above 2 km at noon, therefore, we chose the Sky-surfer X8 (X-UAV) fixed-wing drone with a maximum height of 4 – 5 km, and flight time of 1 – 2 hours with a max payload about 200 g. Throughout the experiment (Ke et al., 2018), the UAV was equipped with a Windsond system (Sparv Embedded AB Company) to measure meteorological parameters, including pressure, temperature, and relative humidity (RH), from which potential temperatures (θ) were calculated to construct the vertical profiles and characterize the PBL structure. The UAV was flown from a site ~2 km north of the sounding station. Before the experiment, quality assessments of the UAV sensors quality assessments were conducted by intercomaprison with a meteorological standard Vaisala RS41 radiosonde launched simultaneously from the Banqiao sounding station, as reported in our previous publication (Ke et al., 2018). We have analyzed the radiosonde data, along with UAV observations in determining PBL height in a previous publication (Ke et al., 2018). The results showed that the UAV system successfully delineated the low-level (0-3 km) atmospheric profile with parameters (temperature,

ACCEPTED MANUSCRIPT

RH, and pressure) in good agreement with the data observed by meteorological radiosondes and MPL, especially for the daytime PBL when the discontinuous layer is associated with an inversion layer easily observed by sounding data. The intercomparison revealed good correlations of temperature ($r > 0.999$) and relative humidity ($r > 0.95$) between the two measurements (Fig. 2). However, a larger difference was observed during the daytime flight suggesting uneven radiation heating of the sensors. Another comparison was made for UAV with Windsond sensor versus balloon with Vaisala RS41 was conducted on August 22 and August 25, 2017 during the measurement period (Fig. 3). To note, the Windsond and Vaisala flight paths were different after launch in this case. The meteorology parameter profiles include air temperature, dew point temperature and RH. Although the flight paths diverged, the results again highlight the reliability of the UAV profile observations, especially for determining the PBLH (~ 920 hPa on August 22, 2017 and ~ 850 hPa on August 25, 2017).

PBLH determined by Gradient method

The gradient method has been applied to determine PBLH in several studies (Boers et al., 1984; Senff et al., 1996). We apply the method to both the volume depolarization ratio from MPL observation and potential temperature from UAV measurements. The gradient method is based on the following differential Eq. (1)

ACCEPTED MANUSCRIPT

$$g(z) = -\frac{d[B(z)]}{dz} \tag{1}$$

where *B(z)* is some range-dependent atmospheric variable (e.g. volume depolarization ratio or potential temperature in this study), *dz* is the vertical resolution of the atmospheric variable, and *g(z)* is the first derivative of *B(z)*. The maximum *g(z)* is the position at the top of the PBL.

Based on the meteorological conditions in the Taipei basin in summer, we assumed that aerosols are mostly distributed beneath the PBL top, thus MPL gradient observation data was used to calculate the PBLH. Considering that the maximum amplitude range of the PBLH should be less than 210 m when using the gradient method (Noonkester et al., 1974; Flamant et al., 1997), the data were averaged for 5 minutes before the gradient calculation. Also, because of near-field limitation (Campbell et al., 1982; Berkoff et al., 2003) we removed the data under 225 m agl (above ground level). In addition, we chose cases on relatively clean days without any long-range transport or transboundary events and with low surface $PM_{2.5}$ concentrations. On these days, it is assumed aerosols were only contributed by local emissions and thus, the range of depolarization ratio could be more easily distinguished. There is usually an inversion layer just above the PBL, so we monitored this with the potential temperature calculated from UAV measurements and compared to the MPL observations.

PBLH determined by δ - threshold method

ACCEPTED MANUSCRIPT

Most locally emitted aerosols originate at the surface. When there is less mixing with transboundary aerosols, PBL aerosols in the Taipei basin are assumed to have similar optical and microphysical properties throughout the PBLH. Thus, we used the volume depolarization ratio (δ_v) to describe diurnal PBLH change. δ_v is provided by the new type-4 polarized MPL systems and can be used to describe the aerosol shape (Flynn et al., 2007). The volume depolarization ratio by MPL is the ratio of the cross-polarized NRB signals and the total (both cross-polarized and co-polarized) NRB signals. From the measurement principle, MPL cannot determine the particle depolarization ratio (δ_p) directly. Other studies have tabulated the relationship between aerosol types and δ_p, where urban aerosol is associated with a δ_p of approximately 0.04, dust with a δ_p approximately 0.3, and other polluted air masses (e.g. biomass burning, sea-salt) are associated with different values (Young, 1982; Müller et al., 2010; Baars et al., 2016), while the Cabannes line suggests a δ_p of approximately 0.004 for pure molecular signal (Young, 1982). According to our measurements in the Taipei basin, δ_v values between 0.028 and 0.032 were considered representative of urban aerosol and used in this study, while any value lower was considered a primary molecular lidar return, thus indicating the free troposphere and delineation of the PBL top. Different sources of aerosol are associated with different depolarization ratio, thus, the threshold may change case by case.

ACCEPTED MANUSCRIPT

PBLH determined by Haar Wavelet Covariance Transform

Wavelet covariance transform (WCT) is a general transform process used to study the characteristics of conditional sampling techniques (Gamage et al., 1993; Senff et al., 1996). WCT has been applied to many scientific research studies (Davis et al., 2000; Brooks et al., 2003) because it can emphasize the magnitude in the signal gradient. WCT is based on Eq. (2)

$$W_f(\Delta h, z_m) = \Delta h^{-1} \int_{z_b}^{z_t} f(z) h\left(\frac{z-z_m}{\Delta h}\right) dz \qquad (2)$$

where *f(z)* is the signal (e.g. lidar volume depolarization ratio profile in our study), z is altitude, z_t and z_b are the top and bottom of the lidar volume depolarization ratio profile, respectively, and h is the mother function of Haar wavelet. We used Haar wavelet (h) defined by Eq. (3). The size of h is determined by z_m the position at which is h centered (translation function), and Δh, the amplitude or spatial scale. This technique uses different combinations of z_m and Δh to arrive at the best results. The location of the maximum value of W_f indicates the altitude of the PBLH.

$$h\left(\frac{z - z_m}{\Delta h}\right) = \begin{cases} -1, for\ z_m - \dfrac{\Delta h}{2} \le z \le z_m \\ 1, \quad for\ z_m \le z \le z_m + \dfrac{\Delta h}{2} \\ 0, \quad for\ elsewhere \end{cases} \qquad (3)$$

ACCEPTED MANUSCRIPT

PBLH determined by Hybrid Image Processing: clustering data by color labeling

Image processing has been used recently in many science and technology applications, including self-driving automobiles, UAVs, artificial intelligence and machine learning. Also, the image processing technique has been applied to find PBLH. Lolli et al. (2011) used the 2D-Sobel algorithm (Sobel et al., 1968) to obtain a gradient image and the PBLH profile by retrieved the range-corrected backscatter signals profile (Lolli et al., 2011). Lewis et al. (2013) used the Canny edge detection algorithm (Canny, 1986) to identify the upper and lower bounds of PBL top features in the Wavelet Covariance Transform (WCT) image (Lewis et al., 2013). Vivone et al. (2020) applied the Morphological Image Processing Approach (MIPA) which performances more stable than the other benchmarking methods and shows a fast running time (Vivone et al., 2020). Our study combines several image processing methods and algorithms into a Hybrid Image Processing method that can detect PBLH and also reduce the noise within the MPL data.

The Hybrid Image Processing method enhances the character of the data through clustering and clearly reveals the diurnal changes. First, we split the depolarization ratio image (Fig. 4(a)) into its three RGB channels (R for red, G for green, and B for blue), and then chose two of the channels to de-saturate and give the best contrast which emphasized the region we need easily (i.e. the area beneath PBL top). Next, we applied a Gaussian filter (Deng and Cahill, 1993) to smooth

ACCEPTED MANUSCRIPT

the color transition and reduce noise. To further decrease noise, we then set up a bi-level threshold (Lucchese and Mitra, 2001) to create a pure black and white image (Fig. 4(b)).

The final and most important step in our image processing is to use the Image Region Segmentation method (Ester et al., 1996) and group the color blocks by neighboring distance relations. In Fig. 4(c), the MPL depolarization ratio profile has been separated into two colors, green and pink, allowing us to easily omit any outliers, consisting of the green points and some higher pink points. The green points represent the noise which is removed, and the pink area represent the aerosols within the PBL. Finally, selected the tip points from the pink area, which indicate the PBLH (Fig. 4(d), light gray points), and applied them back into the original depolarization ratio image (e.g. shown by magenta dots in Fig. 7(c)).

RESULTS AND DISCUSSION

To emphasize the performance of algorithm testing, it is necessary consider cases without too many clouds, a residual layer, or transported pollutants. Due to the rare use of lidar for PBLH determination over subtropical locations, we were seeking to develop the retrieval techniques suitable to these areas for only the best of conditions. Thus, we chose cases less influenced by clouds and transportation events, to ensure the algorithm performed well. Cloudy conditions may

ACCEPTED MANUSCRIPT

be heavily influenced from transported air masses and not dominated by local atmospheric thermodynamics convection, also the boundaries of clouds are difficult to clarify clearly, this may lead unreliable results during PBL detection. Two periods of MPL observations were selected: June 23 – 26, 2017 (Case 1) and August 29, 2017 (Case 2). The meteorological conditions during both periods were suitable for us to do the algorithm testing. The average visibility of these two cases was 20.75 km and 23.07 km, with an average temperature of 30.3 °C and 30.6 °C, and relative humidity of 71.8 % and 66.2 %, respectively. The air quality was fairly clean for a populated area, with mean $PM_{2.5}$ concentrations of 11.0 μg m^{-3} and 6.9 μg m^{-3}, respectively, lower than Taiwan's EPA daily average air quality standard (35.0 μg m^{-3}).

Combining the Gradient and δ-threshold methods and comparing to the WCT

The PBLH retrieval results for Case 1 are shown in Fig. 5. During noontime, clouds contaminated the signal as indicated by the high noise level of δ above the PBL. The results of the Gradient method (Fig. 5(a)) demonstrate that the PBLH estimation was affected by cloud contaminated signals between 11:00 to 14:00, and resulted in an unstable fluctuation. In contrast to the Gradient method, the PBLH retrieved by the δ-threshold method (Fig. 5(b)) shows a more stable daytime pattern than from the Gradient method, indicating the δ-threshold method is less sensitive to and more reliable during the presence of clouds. The δ-threshold method reduces the effect from the clouds around noontime. For the nighttime retrievals, the Gradient method yielded

ACCEPTED MANUSCRIPT

a lower and smoother PBLH compared to the δ-threshold method, suggesting residual layer aerosols may cause the overestimation of nighttime PBLH by the δ-threshold method. Considering the pros and cons of these two methods, we combined them, applying the gradient method results at nighttime (20:00-07:00) and the δ-threshold method results during daytime (07:00 to 20:00), and arrived at a more reasonable solution (Fig. 5(c)).

Continuing with the Case 1 analysis, the Haar wavelet transform exhibited a less noisy retrieval of daytime PBLH (Fig. 6) and was smoother than the results in Fig. 5, but the nighttime PBLH from the Haar wavelet transform was on average 200 meters higher than in the combination result (Fig. 5(c)). The higher nighttime PBLH could be due to a more homogenous aerosol distribution than in daytime, creating difficulties for the Haar wavelet transform method to detect the maximum change of each signal profile. In conclusion to the Case 1 analysis, the Gradient method outperformed the other two methods under nighttime conditions, while the δ-threshold and Haar wavelet methods proved more reliable for the daytime.

Comparison of PBLH evolution from retrievals and UAV measurements

Two-hour routine UAV measurements were only available for Case 2 in this study and thus were included for PBLH comparison. Both the MPL observations and the all-sky images (not shown here) indicate clear sky and low aerosol concentrations during Case 2. On August 29th, we collected seven UAV-profiles performed at local time 06:00, 08:00, 10:00, 12:00, 14:00, 15:30, and 17:30. The θ profiles (blue lines) from the UAV are shown in Fig. 7(c). The values of the

ACCEPTED MANUSCRIPT

PBLH for each flight were 606 m, 636 m, 1226 m, 1445 m, 1379 m, 983 m, and 830 m, respectively (Table 2).

Fig. 7 shows the PBLH retrievals by the combination of the Gradient method and δ-threshold method combination, the Haar wavelet transform, the hybrid image processing, and seven profiles from UAV observations. The method combination was suitable when the PBL had clear development and the asymmetric aerosol distribution decreased with increasing height. However, the δ_v features show larger variability which might be associated with a turbulent boundary layer in this case. The performance of the Gradient method during nighttime largely failed, showing large PBLH variations, while the δ-threshold method showed unreasonably low PBL heights during the daytime (Fig. 7(a)). In addition, the Haar wavelet transform performed better than the previous two methods (Fig. 7(b)), capturing not only the nocturnal boundary layer but also the convective boundary layer during the daytime. The PBLH of each method during the UAV flight time is reported in Table 2. The UAV-derived PBLH was similar to the hybrid image processing result most of the time. The largest differences between them were at 06:00 and 12:00, representing sunrise and local noon, time period and near the peak of active convection.

Table 2 also lists the PBLH difference between each retrieval method and UAV measurements at each flight time on August 29. It shows that the results from these algorithms underestimated the UAV-derived PBLH most of the time. Both the Haar wavelet transform and Hybrid image processing performed well, with the latter was consistently closer to the UAV PBLH results. The PBLH difference between UAV measurements and the Hybrid image processing were 308 and 128 meters at 06:00 and 12:00, respectively. The UAV-derived PBLH is based on observation parameters representing the meteorological state of the atmosphere, while MPL observes the aerosol vertical distribution, thus, the PBLH determinations may not always agree. Uncertainties in the UAV data may have increased with turbulence and influenced the meteorological

ACCEPTED MANUSCRIPT

parameters and thus PBLH estimation. Moreover, the discrepancies between the MPL and UAV methods may be due to complex vertical mixing which can occur during these transition times. For example, the significant changes in solar heating and transportation emissions can introduce variability into the retrievals in the morning hours; at noontime, the boundary between the PBL top and free atmosphere can be more unstable due to solar heating and cloud thermodynamic processes. In this case, we found that cloud dissipation happened around 12:00, which indicates the structure of the inversion layer is breaking up, implying the PBLH retrievals may have greater uncertainty.

CONCLUSIONS

In this study, we used three common algorithms (i.e., the Gradient method, the δ-threshold method, and the Haar wavelet transform), and one new algorithm (the hybrid image processing) to determine the planetary boundary layer height (PBLH) based on aerosol lidar data and compared these results to our observations using a UAV. The experiment was carried out in a subtropical city (New Taipei City, Taiwan) in the summer of 2017. Two cases were selected and studied to understand the effectiveness of using different PBLH retrieval methods and their suitability for the subtropical meteorological conditions.

Our results show that combining the Gradient method and the δ-threshold method can produce better results than using only one of the methods. However, using these two methods may not always be the optimal choice. In general, the performance of the Haar wavelet transform in both cases is better than the PBLH detected by the Gradient method or the δ-threshold method. In Case

ACCEPTED MANUSCRIPT

2, the Haar wavelet showed a better performance than the combined method on a low pollution day. For the PBLH comparison, in Case 2, the temperature inversions monitored by the UAV observation profiles were most consistent with the hybrid image processing method. The vertical aerosol distribution variability caused PBLH discontinuities on both the Gradient method and δ-threshold method. The result of hybrid image processing is consistent with the position of the inversion in the UAV observation. In addition, we must acknowledge the limitations of our study. First of all, our discussions are limited to clean and cloud-free conditions which do not fully represent the gamut of real cases. Second, cloud boundary needs to be more clearly defined. Third, different sources of aerosol are associated with different depolarization ratios; thus, the threshold may change on a case-by-case basis. Finally, at high aerosol concentrations, the boundary between long-range transport or transboundary aerosol and local emissions becomes ambiguous.

The Hybrid Image Processing showed good performance of retrieving PBLHs, and UAV provided a suitable validation technique to verify continuous atmospheric boundary layer observations. Although the novel hybrid image processing technique proved to be highly functional in one scenario, other methods still proved useful under other circumstances (e.g. different times of day, different environmental conditions), and it is suggested that more cases

ACCEPTED MANUSCRIPT

covering more conditions should be analyzed with the suite of retrieval techniques described here and with support of UAV.

ACKNOWLEDGMENTS

We would like to thank NASA MPLNET for their great help with the MPL technology. We would like to thank the Falcon team (falcon.atm.ncu.edu.tw) for their UAV measurement support, Peaceful Pioneer Technology Co. Ltd for providing the technical instrument support, Banqiao sounding weather station for the MPL maintenance support during the campaign. We would like to thank the Ministry of Science and Technology under grant 107-2111-M-008-026. We would like to thank the National Center for High-performance Computing for computer time and facilities, and Ms. Hsiao, who is a member of the Color and Illumination technology group at National Taiwan University of Science and Technology, for providing ideas and discussion on the image processing. Also, we are thankful for the English editing from Mr. Sebastian Stewart, and Mr. Pavel Alam Mushi.

REFERENCES

Baars, H., T. Kanitz, R. Engelmann, D. Althausen, B. Heese, M. Komppula, J. Preißler, M. Tesche, A. Ansmann, and U. Wandinger. (2016). An overview of the first decade of Polly NET: an emerging network of automated Raman-polarization lidars for continuous aerosol profiling.

ACCEPTED MANUSCRIPT

Atmos. Chem. Phys.16(8): 5111-5137.

Berkoff, T., et al. (2003). Investigation of overlap correction techniques for the Micro-Pulse Lidar NETwork (MPLNET). Geoscience and Remote Sensing Symposium. IGARSS'03. IEEE.

Boers, R., Eloranta, E. W., & Coulter, R. L. (1984). Lidar observations of mixed layer dynamics: Tests of parameterized entrainment models of mixed layer growth rate. J. Climate Appl. Meteor. 23(2): 247-266.

Bravo-Aranda, J. A., G. de-Arruda-Moreira, F. Navas-Guzmán, M. Granados-Muñoz, J. Guerrero-Rascado, D. Pozo-Vázquez, C. Arbizu-Barrena, F. Olmo, M. Mallet, and L. Alados-Arboledas. (2017). A new methodology for PBL height estimations based on lidar depolarization measurements: analysis and comparison against MWR and WRF model-based results. Atmos. Chem. Phys. Discuss. 17(11): 6839-6851.

Brooks, I. M. (2003). Finding boundary layer top: Application of a wavelet covariance transform to lidar backscatter profiles. J. Atmos. Ocean. Tech. 20(8): 1092-1105.

Campbell, J. R., D. L. Hlavka, E. J. Welton, C. J. Flynn, D. D. Turner, J. D. Spinhirne, V. S. Scott, and I. H. Hwang. (2002). Full-time, eye-safe cloud and aerosol lidar observation at Atmospheric Radiation Measurement program sites: Instrument and data processing, J. Atmos. Oceanic Technol. 19: 431–442.

ACCEPTED MANUSCRIPT

Canny, J. (1986). A computational approach to edge detection. IEEE Trans. Pattern Anal. Mach. Intell., 8(6): 679-698.

Davis, K. J., N. Gamage, C. Hagelberg, C. Kiemle, D. Lenschow, and P. Sullivan. (2000). An objective method for deriving atmospheric structure from airborne lidar observations. J. Atmos. Ocean. Tech. 17(11): 1455-1468.

De Tomasi, F., M. M. Miglietta, and M. R. Perrone. (2011). The growth of the planetary boundary layer at a coastal site: a case study. Bound.-Lay. Meteorol. 139(3), 521-541.

Deng, G., and L. Cahill. (1993). An adaptive Gaussian filter for noise reduction and edge detection. paper presented at Nuclear Science Symposium and Medical Imaging Conference.

Ester, M., H.-P. Kriegel, J. Sander, and X. Xu. (1996). A density-based algorithm for discovering clusters in large spatial databases with noise. paper presented at Kdd.

Flamant, C., J. Pelon, P. H. Flamant, and P. Durand. (1997). Lidar determination of the entrainment zone thickness at the top of the unstable marine atmospheric boundary layer. Bound.-Lay. Meteorol., 83(2): 247-284.

Flynna, C. J., A. Mendozaa, Y. Zhengb, and S. Mathurb. (2007). Novel polarization-sensitive micropulse lidar measurement technique. Opt. express 15(6): 2785-2790.

Gamage, N., and C. Hagelberg. (1993). Detection and analysis of microfronts and associated

ACCEPTED MANUSCRIPT

coherent events using localized transforms, J. Atmos. Sci. 50(5): 750-756.

Gaudio, P., M. Gelfusa, A. Malizia, S. Parracino, M. Richetta, L. De Leo, C. Perrimezzi, and C. Bellecci. (2015). Detection and monitoring of pollutant sources with Lidar/Dial techniques. J. Phys. Conf. Ser.

He, T.-Y., S. Stanič, F. Gao, K. Bergant, D. Veberič, X.-Q. Song, and A. Dolžan. (2012). Tracking of urban aerosols using combined LIDAR-based remote sensing and ground-based measurements. Atmos. Meas. Tech. 5(5): 891-900.

Hellmann, G. (1915). Uber die Bewegung der Luft in den unterste Schichten der Atmosphare. Meteorol. Z. 34: 273-285.

Ke L.-J., S.-H. Wang*, H.-Y. Huang, Y.-C. Wang, H.-F. Chuang, R.-Y. Hung, Z.-C. You, S.-C. Chang. (2018). Observations on atmospheric boundary layer structure using an unmanned aerial system. J. Photogramm. Remote Sensing, 23: 103-113. (in Chinese)

Lewis, J. R., E. J. Welton, A. M. Molod, and E. Joseph. (2013). Improved boundary layer depth retrievals from MPLNET. J. Geophys. Res. Atmos.118(17): 9870-9879.

Lolli, S., R. Delgado, J. Compton, and R. Hoff. (2011). Planetary boundary layer height retrieval at UMBC in the frame of NOAA/ARL campaign. Lidar Technologies, Techniques, and Measurements for Atmospheric Remote Sensing VII, International Society for Optics and

ACCEPTED MANUSCRIPT

Photonics.

Li, H., Y. Yang, X. M. Hu, Z. Huang, G. Wang, B. Zhang, and T. Zhang. (2017). Evaluation of retrieval methods of daytime convective boundary layer height based on lidar data. J. Geophys. Res. Atmos. 122(8): 4578-4593.

Lucchese, L., and S. K. Mitra. (2001). Colour image segmentation: a state-of-the-art survey. Proceedings-Indian National Science Academy Part A 67(2): 207-222.

Mildner, P. (1932). Uber Reibung in einer speziellen Luftmasse. Beitr. Phys. Fr. Atmos. 19: 151-158.

Müller, D., B. Weinzierl, A. Petzold, K. Kandler, A. Ansmann, T. Müller, M. Tesche, V. Freudenthaler, M. Esselborn, and B. Heese. (2010). Mineral dust observed with AERONET Sun photometer, Raman lidar, and in situ instruments during SAMUM 2006: Shape-independent particle properties. J. Geophys. Res. Atmos. 115(D7).

Noonkester, V., D. Jensen, J. Richter, W. Viezee, and R. Collis. (1974). Concurrent FM-CW radar and lidar observations of the boundary layer. J. Appl. Meteorol. 13(2): 249-256.

Peppler, A. (1921). Windmessungen auf dem Eilveser Funkenturm. Beitr. Phys. Fr. Atmos. 9: 114-129.

Senff, C., J. Bo¨ senberg, G. Peters, and T. Schaberl. (1996). Remote sensing of turbulent ozone

ACCEPTED MANUSCRIPT

fluxes and the ozone budget in the convective boundary layer with DIAL and Radar-RASS: A case study. Contrib. Atmos. Phys. 69: 161–176.

Sobel, I., Feldman, G. (1968). A 3 × 3 isotropic gradient operator for image processing. Presented at a talk at the Stanford Artificial Project.

Spinhirne, J. D. (1993). Micro pulse lidar. IEEE Transactions on Geoscience and Remote Sensing 31(1): 48-55.

Stull, R. B. (1988). An introduction to boundary layer meteorology. Springer Science & Business Media.

Vivone, G., G. D'Amico, D. Summa, S. Lolli, A. Amodeo, D. Bortoli, and G. Pappalardo. (2020). Atmospheric Boundary Layer height estimation from aerosol lidar: a new approach based on morphological image processing techniques. Atmos. Chem. Phys. Discussions, 1-37.

Welton, E. J., K. J. Voss, P. K. Quinn, P. J. Flatau, K. Markowicz, J. R. Campbell, J. D. Spinhirne, H. R. Gordon, and J. E. Johnson. (2002). Measurements of aerosol vertical profiles and optical properties during INDOEX 1999 using micropulse lidars. J. Geophys. Res. Atmos 107(D19).

Welton, E. J., and J. R. Campell. (2002). Micro-pulse Lidar Signals: Uncertainty Analysis. J. Atmos. Oceanic Technol. 19, pp. 2089-2094.

ACCEPTED MANUSCRIPT

Welton, E. J., S. Stewart, J. R. Lewis, L. Belcher, J. R. Campbell, and S. Lolli. (2018). Status of the NASA Micro Pulse Lidar Network (MPLNET): overview of the network and future plans, new version 3 data products, and the polarized MPL. EPJ Web of Conferences. 176.

Young A. T. (1982). Rayleigh scattering. Phys. Today. 42–48.

ACCEPTED MANUSCRIPT

Table 1. The specifications of Type-4 MPL.

Transmitter	
Laser wavelength	532 nm
Laser Pulse Frequency	2500 Hz
Laser Pulse Energy	6 – 8 μJ
Receiver	
Telescope Type	Maksutov Cassegrain
Focal Length	2400 mm
Diameter	178 mm
Field of View	100 μrad
Data System	
Detector	Avalanche APD, photon counting mode
Range resolution	5/ 15/ 30/ 75 m (programmable)
Temporal resolution	Minimum: 1 s (programmable)
Maximum range	45 km

Table 2. The PBLH retrievals and differences between each retrieval method and UAV-derived result at each flight times on August 29.

	Time (LT)						
	06:00	08:00	10:00	12:00	14:00	15:30	17:30
Methods (Difference)	PBLH (meter)						
UAV	606	636	1226	1445	1379	983	830
Combination	554 (-52)	824 (188)	861 (-365)	388 (-1057)	774 (-605)	680 (-303)	375 (-455)
Haar wavelet transform	295 (-311)	596 (-40)	1054 (-172)	1328 (-117)	1028 (-351)	1143 (-160)	459 (-371)
Hybrid image processing	300 (-306)	635 (1)	1225 (-1)	1575 (130)	1340 (-39)	995 (12)	840 (10)

ACCEPTED MANUSCRIPT

Figure Captions

Fig. 1. (a) Population map of Taiwan; (b) locations of Banqiao sounding / MPL station (24.99°N, 121.44°E) and UAV flight site (25.02°N, 121.44°E) in the Taipei basin.

Fig. 2. The correlation between the Vaisala RS41 radiosonde and the Windsond system. R values indicate the correlation coefficients. (a)-(b) November 9, 2017 (08:00 LT); (c)-(d) November 27, 2017 (20:00 LT). (a) and (c) temperature (°C, blue dots); (b) and (d) relative humidity (%, green dots).

Fig. 3. Comparison of UAV measurements and Sounding observations on August 22, 2017 (08:00 LT, (a)-(b)) and August 25, 2017 (11:00 LT, (c)-(d)). For the temperature and RH plots, the blue lines and the brown lines represent the data collected by UAV and Sounding, respectively. For the dewpoint, the light blue lines and orange lines represent the results calculated from the data of UAV measurements and Sounding measurements, respectively.

Fig. 4. An example for clustering data by color labeling. (a) The depolarization ratio measurement by MPL on August 29, 2017 at Banqiao station; (b) Bi-level thresholding; (c) Image region segmentation; (d) Locating the tip points.

Fig. 5. The retrieval results of Case 1. (a) Gradient method; (b) δ-threshold method; (c) Combination of Gradient method (purple dot) and δ-threshold method (magenta dot).

Fig. 6. The retrieval result from the Haar wavelet transform of Case 1. The light brown area represents the region within the PBL. Therefore, the upper edge of this area is the PBL top.

Fig. 7. Comparison of the PBLH by using different methods in Case 2. (a) Combining the Gradient method (in purple dot), and δ-threshold method (in magenta dot); (b) Haar wavelet transform; (c) θ profile from UAV measurements; the PBLH calculated from this profile is shown as short-horizontal blue lines, and the result of hybrid image processing as pink dot.

ACCEPTED MANUSCRIPT

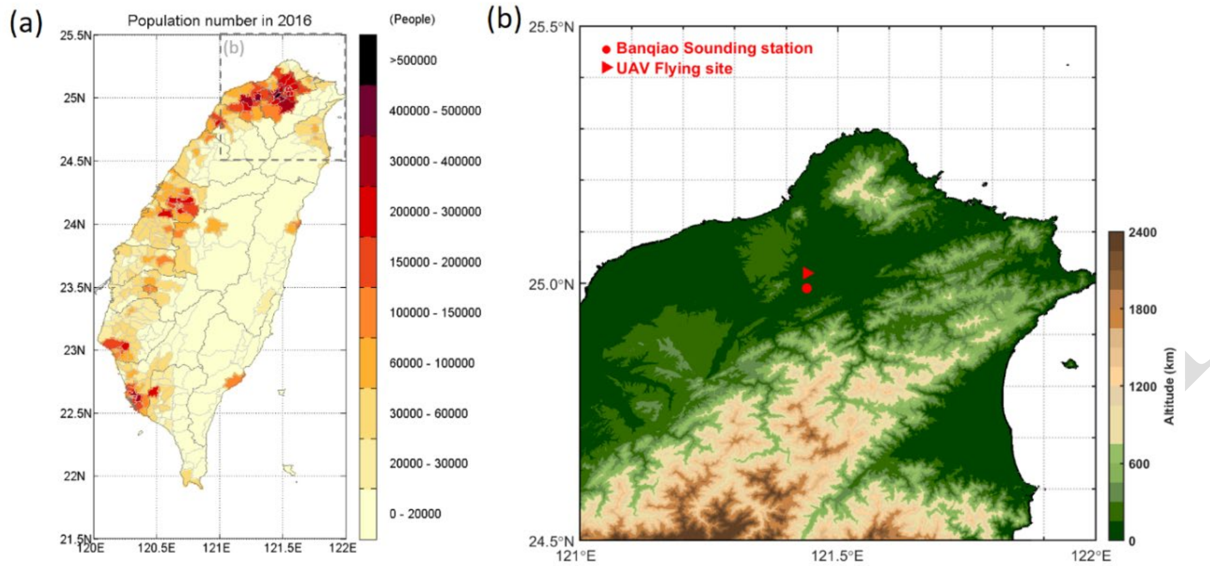

Fig. 1. (a) Population map of Taiwan; (b) locations of Banqiao sounding / MPL station (24.99°N, 121.44°E) and UAV flight site (25.02°N, 121.44°E) in the Taipei basin.

ACCEPTED MANUSCRIPT

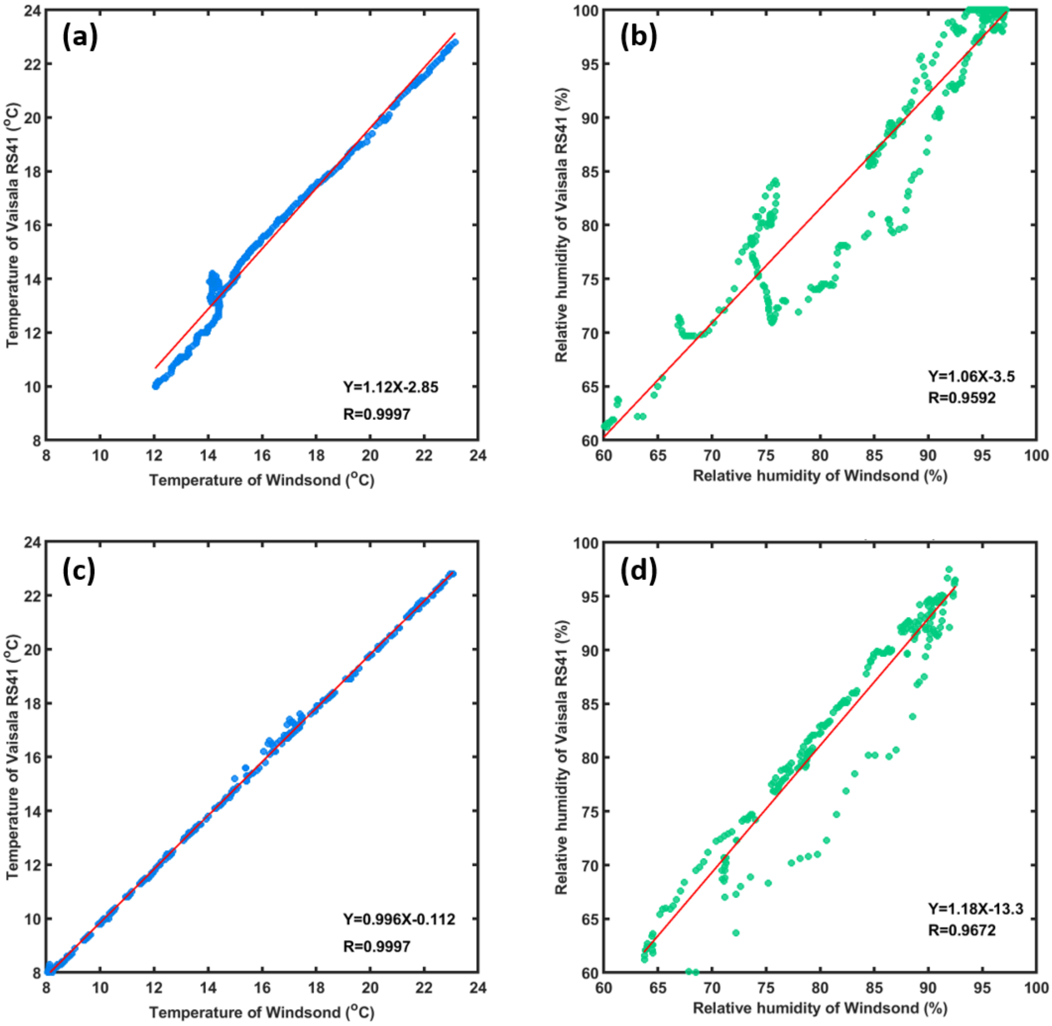

Fig. 2. The correlation between the Vaisala RS41 radiosonde and the Windsond system. R values indicate the correlation coefficients. (a)-(b) November 9, 2017 (08:00 LT); (c)-(d) November 27, 2017 (20:00 LT). (a) and (c) temperature (°C, blue dots); (b) and (d) relative humidity (%, green dots).

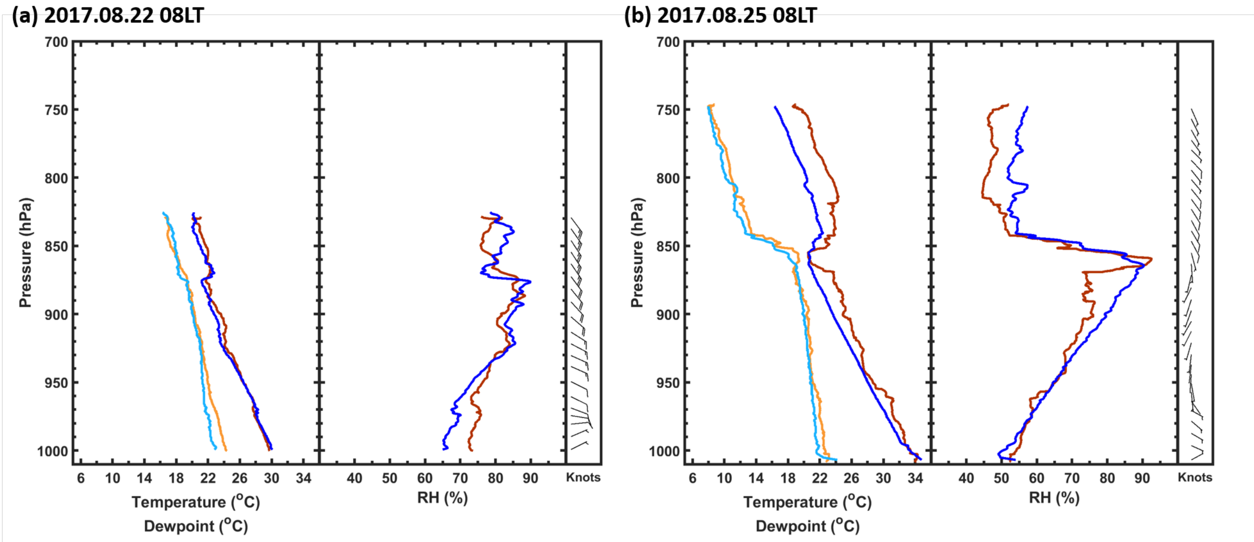

Fig. 3. Comparison of UAV measurements and Sounding observations on August 22, 2017 (08:00 LT, (a)-(b)) and August 25, 2017 (11:00 LT, (c)-(d)). For the temperature and RH plots, the blue lines and the brown lines represent the data collected by UAV and Sounding, respectively. For the dewpoint, the light blue lines and orange lines represent the results calculated from the data of UAV measurements and Sounding measurements, respectively.

ACCEPTED MANUSC

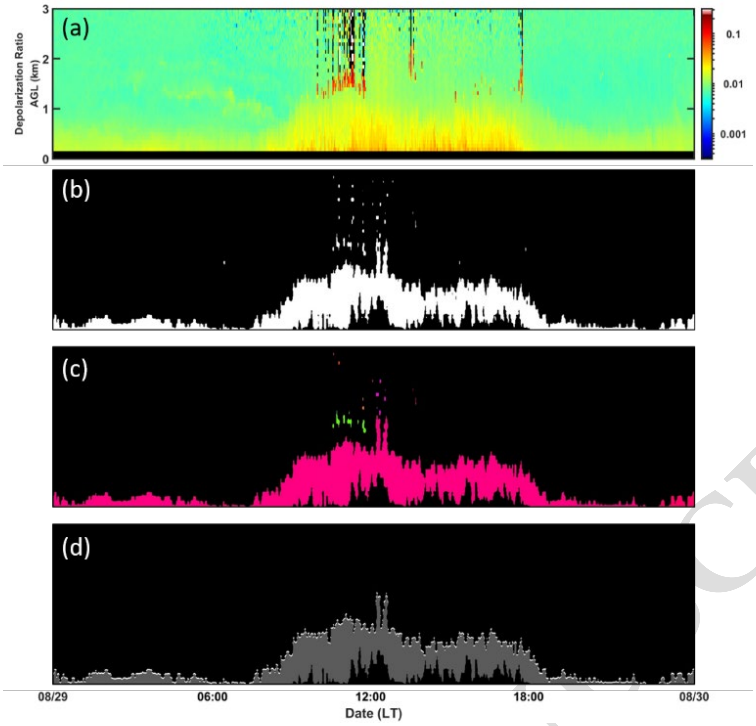

Fig. 4. An example for clustering data by color labeling. (a) The depolarization ratio measurement by MPL on August 29, 2017 at Banqiao station; (b) Bi-level thresholding; (c) Image region segmentation; (d) Locating the tip points.

ACCEPTED MANUSCRIPT

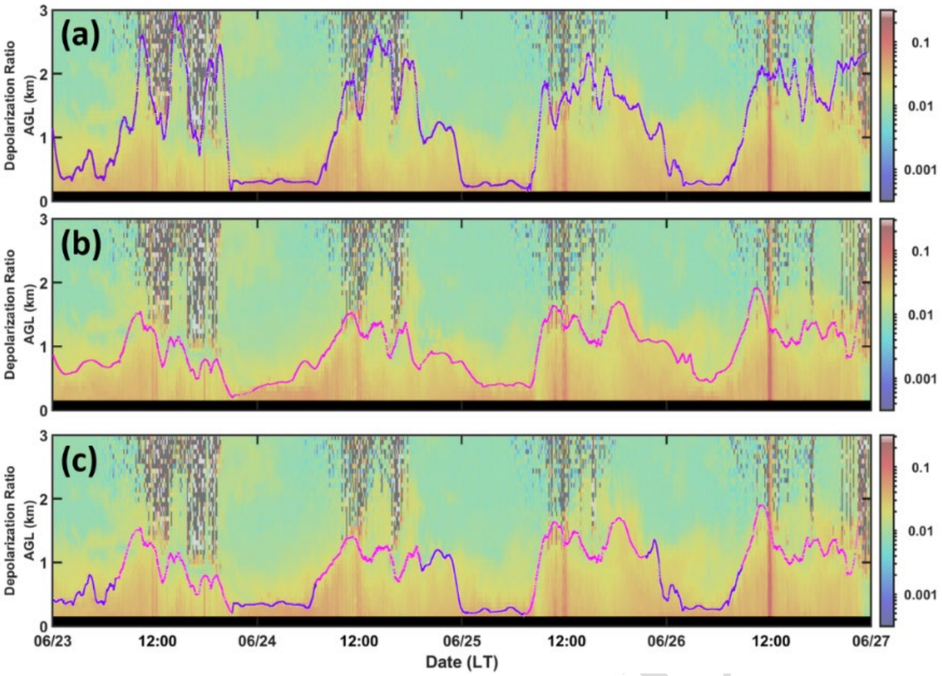

Fig. 5. The retrieval results of Case 1. (a) Gradient method; (b) δ-threshold method; (c) Combination of Gradient method (purple dot) and δ-threshold method (magenta dot).

ACCEPTED MANUSCRIPT

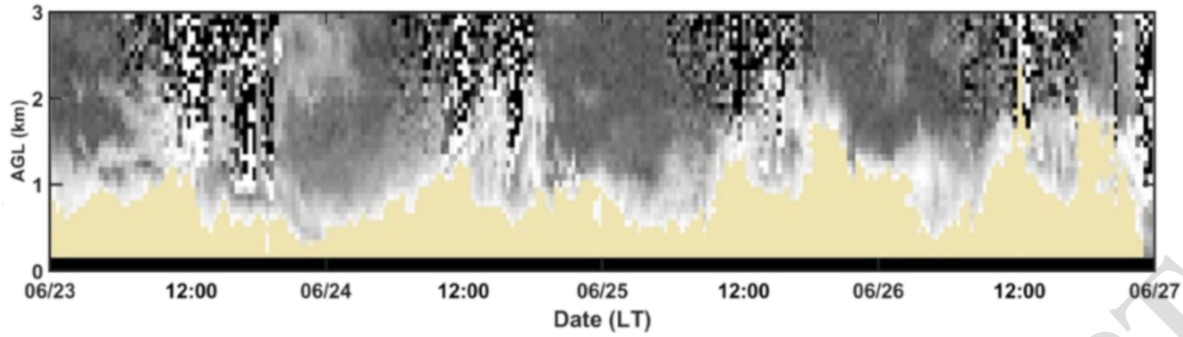

Fig. 6. The retrieval result from the Haar wavelet transform of Case 1. The light brown area represents the region within the PBL. Therefore, the upper edge of this area is the PBL top.

ACCEPTED MANUSCRIPT

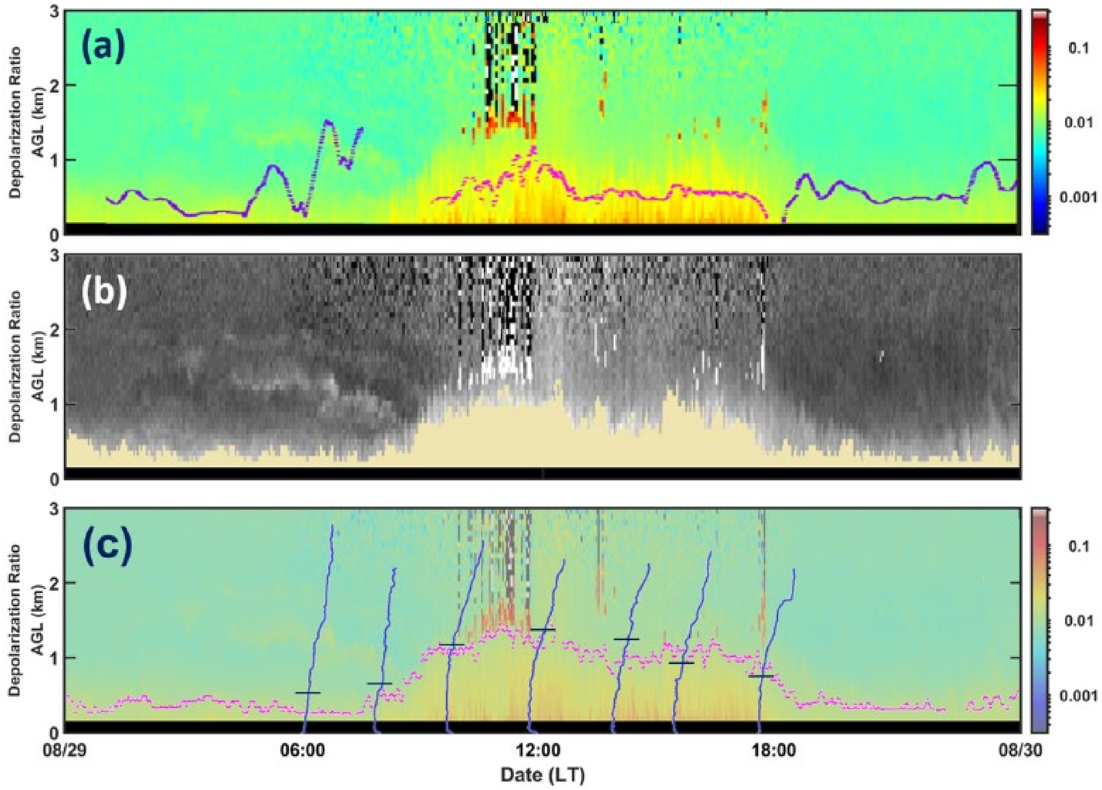

Fig. 7. Comparison of the PBLH by using different methods in Case 2. (a) Combining the Gradient method (in purple dot), and δ-threshold method (in magenta dot); (b) Haar wavelet transform; (c) θ profile from UAV measurements; the PBLH calculated from this profile is shown as short-horizontal blue lines, and the result of hybrid image processing as pink dot.